Journal of Engineering Physics and Thermophysics, Vol. 79, No. 3, 2006

MATHEMATICAL SIMULATION OF A SUPERSONIC FLOW AROUND COMPLEX OBJECTS. INFLUENCE OF THE POSITION OF A WING ON THE GASDYNAMIC CHARACTERISTICS OF A COMPLEX OBJECT

V. F. Volkov

UDC 518.4:533.4:629.7

Results of numerical simulation of a supersonic flow around spatial configurations of flying vehicles with the use of the Euler equations are presented. A model of a complex object was constructed on the basis of simpler base objects. Results of numerical solution of the problem on a three-dimensional flow around objects with an ogival-cylindrical airframe and a triangular wing with a diamond-shaped profile, arranged in different ways, at a Mach number $M_\infty = 4.03$ and an angle of attack $\alpha = 10.1^o$ have been analyzed. Calculation data were compared with the analogous data of a physical experiment.

The main point in the deviation of an algorithm for calculating three-dimensional flows in the neighborhood of different-configuration objects in problems of aerodynamics is the construction of a geometric model of the object being studied. A model of a complex object can be constructed using base objects [1–3]. In problems of aerodynamics, such objects are an airframe, wings, and stabilizers. Base objects are represented by blocks of subprograms, in which the geometry of an object is described by using high-level programming means and the mathematical apparatus of analytical geometry. A characteristic feature of this method is that the necessary requirements for the compactness and openness of program blocks are met when analytical expressions defining the geometry of an object are selected appropriately. At the initial stage of search for an aerodynamic geometry of an object, the indicated method allows one to perform extensive parametric numerical investigations of the gas dynamics of a flow in the neighborhood of this object.

In the present work, a supersonic flow around a complex object with a cylindrical airframe with an ogival head and a triangular wing with a diamond-shaped profile was investigated. A supersonic flow around this object with different arrangements and geometries of the frame and triangular wing were calculated at $M_\infty = 4.03$ and $\alpha = 10.1^o$ of an incident flow. The results obtained were compared with the analogous results of a physical experiment.

Description of the Geometry of an Airframe. The cross sections of the airframe of the object considered represent plane hyperellipses [1, 3]. The elliptic and prismatic axisymmetric bodies are described in the longitudinal direction in the cross sections x = const by a hyperbolic function. In the cylindrical coordinate system $y = r \cos(\varphi)$, $z = r \sin(\varphi)$, this function, in the implicit form $F(x, r, \varphi) = 0$, is as follows:

$$F(x, r, \varphi) = r\left(\cos^n \varphi + \mu^n \sin^n \varphi\right)^{1/n} - \mu a = 0 . \quad (1)$$

The exponent n determines the cross-section configuration of the body. In the equation for an ellipse with semi-axes a and b, $n = 2$. This expression defines a fairly wide class of conic configurations with different n and the ratio between the semi-axes $\mu = b/a$. Here, a is a semi-axis in the direction of the z axis — a function of x in the general case. For example, for a conic head, $a = \tan\theta\, x$, where θ is a half-angle of a cone. The surface of the airframe is defined, in the general case, with the use of the functional dependences of the semi-axes $a = a(x)$ and $b = b(x)$.

Institute of Theoretical and Applied Mechanics, Siberian Branch of the Russian Academy of Sciences, 4/1 Institutskaya Str., Novosibirsk, 630090, Russia; email: volkov@itam.nsc.ru. Translated from Inzhenerno-Fizicheskii Zhurnal, Vol. 79, No. 3, pp. 47–55, May–June, 2006. Original article submitted August 11, 2004; revision submitted April 1, 2005.

1062-0125/06/7903-0467

Geometry of a Triangular Wing with a Diamond-Shaped Profile. The geometry of a triangular wing with a pointed leading edge and a plane middle surface is defined by the following relations:

$$y = \pm C_{\text{w}} (x - x_k) \tag{2}$$

at $x \le (x_i + x_k)/2$ and

$$y = \pm C_{\text{w}} (x_i - x) \tag{3}$$

at $x > (x_i + x_k)/2$.

The coefficient C_{w} is determined by the thickness of the profile and is equal to C_{up} for the upper part of the wing ($y > 0$) and C_{low} for its lower part ($y < 0$). In the particular case of a symmetric profile, $C_{\text{w}} = C_{\text{up}} = C_{\text{low}}$. This wing with a symmetric diamond-shaped profile along the local chord has a sweep angle $\chi = 70.67^{\text{o}}$ and $C_{\text{w}} = 0.3$ at $z = \text{const}$.

Construction of a Geometric Model of a Complex Object. A geometric model of a complex object is constructed on the basis of simpler base objects. In this model, the line of intersection of components of this object — an airframe, a wing, and an empennage — is determined. This line represents a solution of the system of equations for the indicated components of the complex-geometry object considered. In the case where the cross section $x_k = \text{const}$, this system consists of Eqs. (1)–(3). Equations (2) and (3) in the form $y = \psi[(x_k - x_{\text{w}}), (z - z_k)]$ define the profile of the wing. Here, x_{w} is the coordinate of the origin of the board chord of the wing, determining the position of the wing on the airframe. The system of equations (1)–(3) determines the line of intersection of the airframe with the wing and is solved by the Newton iteration method [1]. The coordinates of the profile of the root chord of the wing, determined by the relation $y_k = \psi[(x - x_{\text{w}}), 0]$, can serve as the initial approximation at a current value of x.

For construction of the geometry of the complex object considered, it is necessary to know the values of x of the longitudinal coordinates determining the positions of the plane of conjugation of the components of this object and the cross section $x = \text{const}$ at the characteristic points.

Formulation of the Problem. A supersonic three-dimensional flow of a compressible viscous gas around a complex object at $M_\infty > 1$ is considered. The problem is solved in a region bounded by the surfaces of the object and a leading shock wave.

The nonstationary motion of a compressible gas in any finite volume inside a disturbed region, where sources and sinks are absent, is defined by the equation [4, 5]

$$\iiint_{\Omega} \frac{\partial f}{\partial t}\, d\Omega + \iint_{S} \mathbf{F}(g)\, d\mathbf{S} = 0\,, \quad f = \begin{Bmatrix} \rho \\ \rho v_x \\ \rho v_y \\ \rho v_z \\ E \end{Bmatrix}, \quad \mathbf{F}(g) = \begin{Bmatrix} \rho \mathbf{w} \\ \rho v_x \mathbf{w} + p\mathbf{i} \\ \rho v_y \mathbf{w} + p\mathbf{i}_2 \\ \rho v_z \mathbf{w} + p\mathbf{i}_3 \\ (E + p)\,\mathbf{w} \end{Bmatrix}.$$

The pressure is determined from the equation of state that closes the system and, for an ideal gas, has the form $p = (\gamma - 1)\rho e$.

The computational region is divided into nonintersecting volumes. Approximate initial equations are constructed for each elementary volume and the gas-dynamic parameters on the faces of cells are determined linearly by their values at the nodes. The problem on a stationary flow with a definite initial field around the object is solved in each cross section $x = \text{const}$. In this case, the parameters of the flow in the first marching cross section are calculated if the flow in the neighborhood of the point nose of the object is conical [5]. In the process of solution, the position of the leading shock wave is corrected. The boundaries of the computational region are the surface of the leading shock wave at which the parameters of the flow in the perturbed region are related to the parameters of the incident flow by the Rankine–Hugoniot relations, the surface of the body on which the nonpercolation conditions are fulfilled, the condition of symmetry of the flow in the case where an object has a symmetry plane, and the condition of matching of solution in the $x0y$ plane in the case of a slip flow. The nonpercolation condition was provided for the pointed edge, when the vector of the normal to it was known, by a standard procedure [6, 7].

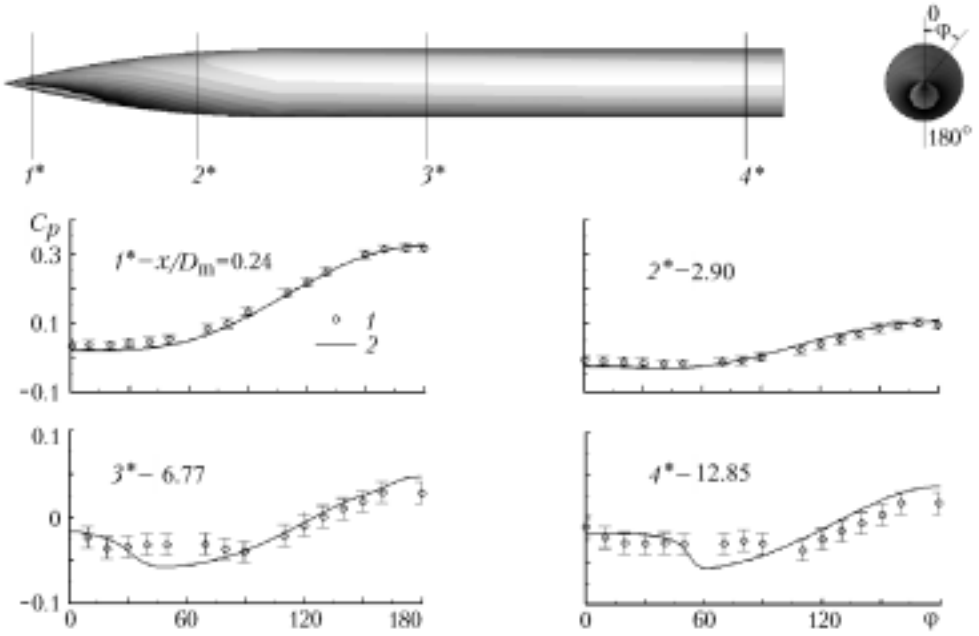

Fig. 1. Distribution of the pressure coefficient in the cross sections of an air frame: 1) experiment; 2) calculation.

The numerical algorithm proposed allows one to solve the problem formulated with separation of a leading shock wave or by the through method. In the first case, the location of the leading shock wave is determined at each iteration time step and the problem is solved on an adaptive grid. In the second case, calculation is carried out using a fixed grid and the parameters of an incident flow are determined at the outer boundary.

Flow around an Isolated Airframe. An isolated airframe represents a combination of axisymmetric bodies. It consists of a head ogival part with an elongation $\lambda_h = 4$ and a cylinder with an elongation $\lambda_c = 9.7$. Calculation was performed for an incident flow with $M_\infty = 4.03$ and $\alpha = 10.1^o$ with separation of the leading shock wave.

In the process of analysis of the gas-dynamic structure of the flow in the neighborhood of the body studied, some characteristic regions were considered. As a criterion of separation of these regions, the value of the cosine of the angle between the velocity vector of the incident flow and the outer normal to the surface of the body at each of its points, i.e., cos $(\mathbf{w}_\infty\mathbf{n}) = \mathbf{w}_\infty\mathbf{n}$, was used. For the flow regime considered, two characteristic regions can be separated in the neighborhood of the body around which a stream flows. The first of them is the upstream side of the body, where $\pi/2 < \varphi < \pi$. Here, cos $(\mathbf{w}_\infty\mathbf{n}) \le 0$ and the distribution of the pressure coefficients C_p in the cross sections x = const is a monotonically increasing function with a maximum on the generating line $\varphi = \pi$ (Fig. 1). The second region is the downstream side of the body $0 < \varphi < \pi/2$. This region, in turn, can be divided into subregions by the value of cos $(\mathbf{w}_\infty\mathbf{n})$ — regions "visible" and "invisible" for the incident flow. The "visible" subregion, where cos $(\mathbf{w}_\infty\mathbf{n}) \le 0$, arises in the flow regime considered in the leading ogival part of the airframe at $0 \le x/D_m < 2.9$. Here, in the cross sections of a part of the body, the pressure-coefficient distribution represents a monotonically increasing function with a maximum on the generating line $\varphi = \pi$ lying on the upstream side and a minimum on the downstream side at $\varphi = 0$ [8]. It is seen from Fig. 1 that the distribution of $C_p(\varphi)$ in cross sections 1^* and 2^* is monotone in character and that the calculation data are in good agreement with the experimental ones [9].

In the case considered, the subregion "invisible" for the incident flow, where cos $(\mathbf{w}_\infty\mathbf{n}) > 0$, includes a part of the ogival head surface and the downstream surface of the cylinder at $x/D_m > 2.9$. This region is responsible for the formation of a flow with a complex gas dynamics on the downstream side. Here, a negative pressure gradient is formed, i.e., $\partial C_p(\varphi)/\partial\varphi < 0$; the reason for this gradient is an intensive stream flowing from the upstream side to the downstream side and a decrease in the transverse component of the velocity vector in the neighborhood of the symmetry plane of the body. This feature is shown in Fig. 1 for cross sections 3^* and 4^* in the cylindrical part of the body. Under actual conditions, this gradient causes a separation of the boundary layer that is not reproduced in the process of numerical solution of the problem within the framework of the Euler equations. At $M > 1$, due to the

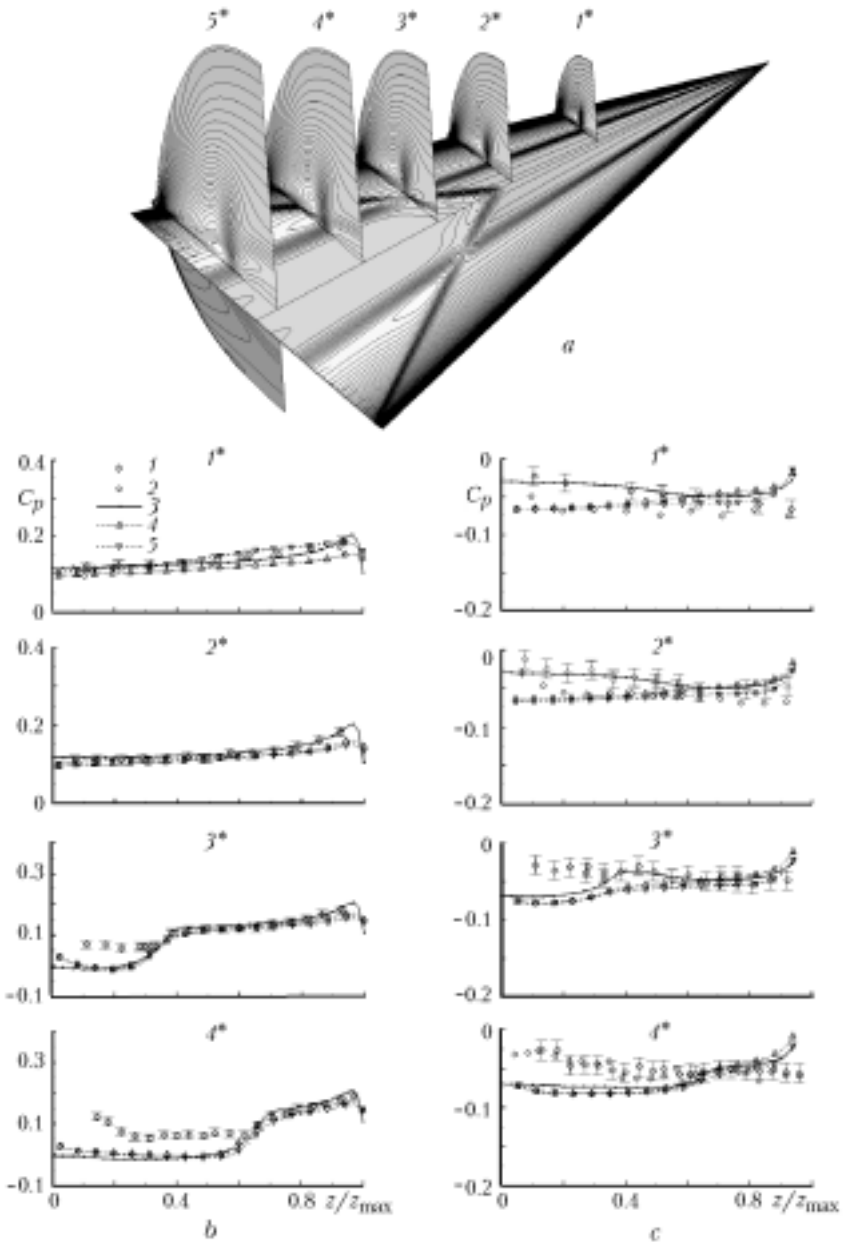

Fig. 2. Distribution of the pressure coefficient in the cross sections of a wing: a) isoMachs in the neighborhood of the wing; b) upstream surface of the wing; c) downstream surface of the wing. Isolated wing: 1) experiment; 3) calculation. Wing in the presence of an airframe: 2) experiment; 4, 5) calculation at $x_w = 4D_m$ and $6.8D_m$ respectively.

pressure gradient, a longitudinal jump arises in the transverse velocity component on the downstream side of the body [10].

Comparison of the calculated values of $C_p(\varphi)$ in cross sections 3^* and 4^* with the experimental data of [9] have shown that these data differ mainly in the region of boundary-layer separation at $30^o < \varphi < 80^o$ (Fig. 1).

Flow around an Isolated Wing with a Diamond-Shaped Profile. The problem on a flow around an isolated triangular wing with a sweep angle $\chi = 70.67^o$ was solved for an incident flow with $M_\infty = 4.03$ and $\alpha = 10.1^o$ with separation of the leading shock wave. The results of calculation of an isolated wing are presented in Fig. 2. The distributions of the pressure coefficients $C_p(\bar{z})$ over the wing span in the cross sections x = const are shown in Fig. 2b

and c: $x = 32b_0$ (1^*), $0.47b_0$ (2^*), $0.62b_0$ (3^*), $0.76b_0$ (4^*), and $0.92b_0$ (5^*). Here, $\bar{z} = z/z_{max}$ is a relative spanwise coordinate; the coordinates of the cross sections were selected in accordance with experimental data.

The character of flow around an isolated triangular wing is determined by the velocity of the incident flow, the angle of attack, and the thickness of the wing; various flow regimes can be realized depending on the indicated parameters especially on the downstream side of the body considered [9]. For the flow regime investigated, $M_n = M_\infty \sqrt{1 - (\sin \chi \cos \alpha)^2} > 1$, i.e., the flow around the leading edge is supersonic, and, as calculations show, the leading shock wave attaches to the edge with the formation of an internal compression shock on the downstream side of the body [7]. In the case represented in Fig. 2a, the leading shock wave in cross sections 1^*–5^* bounds the disturbed region. The calculated distributions of the Mach number on the downstream side of the wing surface and in the disturbed flow, shown in Fig. 2a, point to the formation of an internal compression shock. Figure 2b and c shows the spanwise distributions of the pressure coefficients $C_p(\bar{z})$ in different cross sections. On the whole, the change in the distribution of $C_p(\varphi)$ on both the upstream (Fig. 2b) and downstream (Fig. 2c) sides of the wing, arising when passing from section to section to the line of maximum thickness of the wing, corresponds to a canonical flow.

The distribution of $C_p(\bar{z})$ in cross sections 1^* and 2^* ($x < 0.5b_0$) at the upstream surface is a monotonically increasing function, i.e., the pressure increases from the root chord ($\bar{z} = 0$) to the leading edge of the wing ($\bar{z} = 1$). The flow in the cross sections $x < 0.5b_0$ positioned on the line of maximum thickness of the wing expands in the longitudinal and transverse directions, with the result that the pressure decreases sharply. The pattern of the spanwise pressure distributions in cross sections 3^* and 4^* is substantially deformed because of the profiling of the wing. This feature follows from both the calculation and experimental data presented in Fig. 2b; it is seen that these data are in good agreement. The observed difference between the indicated data obtained for the near-edge region is local in character and is explained by the strong irregularity of the finite-difference grid under the conditions of attachment of the bow shock to the leading edge. The conical bulge on the wing, necessary for attachment of a holder in experiments, disturbs the pattern of pressure distribution over the wing surface. This explains the existence, at $\bar{z} \le 0.3$, of an increased-pressure region in cross section 4^* in the indicated experiments.

In the cross sections on the downstream side of the wing there arises a flow directed from the leading edge $\bar{z} = 1$ to the symmetry plane of the wing $\bar{z} = 0$. A stagnation of the flow in the neighborhood of the symmetry plane of the wing leads to the appearance of a positive pressure gradient $\partial C_p(\bar{z})/\partial\bar{z} > 0$ that, at a supersonic velocity of the transverse flow in the neighborhood of the leading edge, gives rise to the formation of an internal longitudinal compression shock, which is seen from Fig. 2a. The existence of an internal shock in a flow is evidenced by the increased density of the isolines in cross sections 1^*–5^*, and a track of this shock on the surface has the form of a straight line with origin at the top of the wing.

Comparison of calculation and experimental data obtained for the downstream side of the wing has shown that the calculated distributions of $C_p(\bar{z})$ in cross sections 1^* and 2^* (Fig. 2c) agree fairly well with the corresponding data of a physical experiment. However, the decreased experimental value of the gradient $\partial C_p(\bar{z})/\partial\bar{z}$ and the difference between the calculated and experimental values of C_p in the neighborhood of the root chord are explained by the influence of the boundary layer, which was not taken into account in the calculations. This effect manifested itself most pronouncedly in cross sections 3^* and 4^* (Fig. 2c).

Flow around an Object Composed of a Triangular Wing and an Ogival-Cylindrical Airframe. An "airframe + wing" object is obtained by combination of the above-described elements. The position of the wing on the airframe is determined by the coordinate of the bort-chord $x_w = x/D_m$ that is measured from the point nose of the airframe. At $x_w = 4D_m$, the origin of the bort chord coincides with the coordinate of conjugation of the ogival part of the airframe with the cylinder (Fig. 3a, object 1), and $x_w = 6.8D_m$ corresponds to the coincidence of the trailing edge of the wing with the bottom section of the cylindrical part of the frame (Fig. 3b, object 2). The calculations were carried out with separation of the leading shock wave. Figure 3 shows the geometry of the objects considered, the configuration of the leading shock wave, and the results of calculations of the distributed loads on the surface of the bodies in the form of pressure-coefficient isolines. In the case of an incident flow with definite parameters, the whole wing is in a disturbed region bounded by the leading shock wave generated by the airframe, and the flow around the wing, arising in the neighborhood of the airframe, is nonuniform.

The spanwise distributions of the pressure coefficients in the cross sections of the wing in the presence of the airframe are presented in Fig. 2. The cross sections selected correspond to the cross sections of an isolated wing.

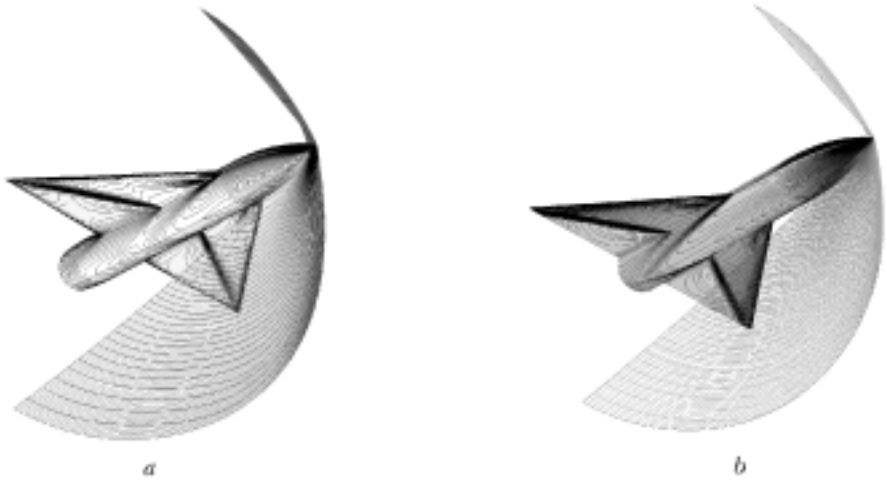

Fig. 3. Scheme of a flow around object 1 at $x_w = 4D_m$ (a) and object 2 at $x_w = 6.8D_m$ (b).

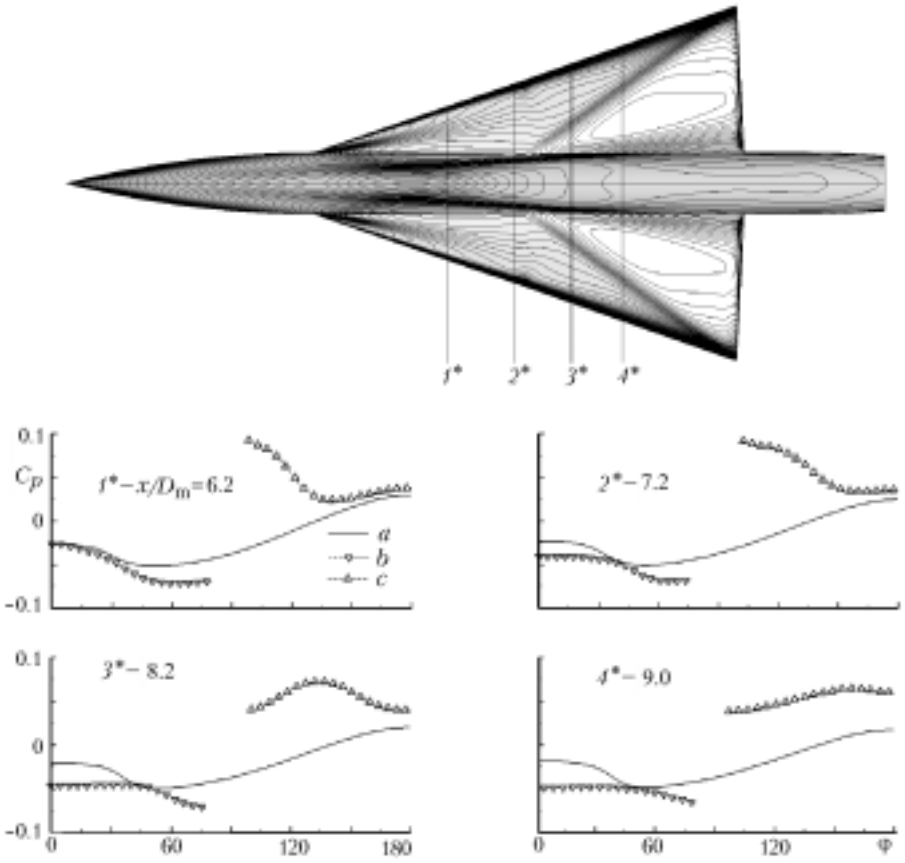

Fig. 4. Distribution of the pressure coefficient in the cross sections of the airframe of object 1 ($x_w = 4D_m$): a) isolated airframe; b) downstream side; c) upstream side.

The results presented show that there is a qualitative analogy between the $C_p(\bar{z})$ distributions of the isolated wing and the wing in objects 1 and 2 with an airframe. However, in the wing cross section 1^* on the upstream side of object 1 (Fig. 2b), the value of $C_p(\bar{z})$ is increased, which can be explained by the nonuniformity of the flow induced by the head part of the body. The rarefaction arising in the neighborhood of the bourd chord on the downstream

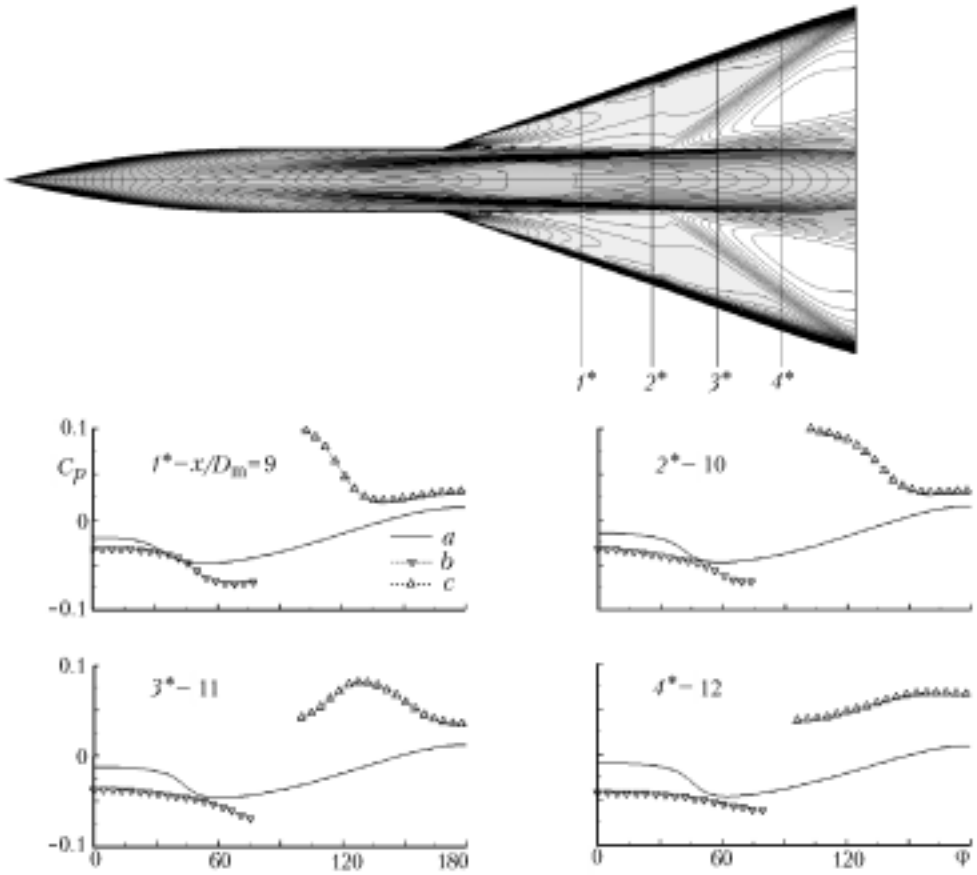

Fig. 5. Distribution of the pressure coefficient in the cross sections of the airframe of object 2 (x_w = 6.8D_m): a) isolated airframe; b) downstream side; c) upstream side.

side of the wing, forming a system with the airframe, is stronger than that of the isolated wing. This feature for cross sections 1^* and 2^* is shown in Fig. 2c. The distributions of $C_p(\bar{z})$ over the wing panel, in the region located closer to the leading edge, are practically coincident. The calculation data (see Fig. 2) show that the point of conjugation of the wing with the airframe does not influence the distributed loads on the wing, which is in agreement with experimental data [9].

The local loads $C_p(\varphi)$ in the cross section x/D_m = const of the isolated airframe and of the airframes of objects 1 and 2 are presented in Figs. 4 and 5. Here, the cross sections selected correspond to the cross sections of the isolated wing. An impression of the main changes arising in a flow around the airframe in the presence of the wing can be gained from the comparison of the distribution of $C_p(\varphi)$ over the surface of the isolated airframe with the analogous distribution over the airframe with the wing.

Such a comparison is presented in Figs. 4 and 5, where the distributions of $C_p(\varphi)$ are given for the isolated airframe and for the downstream and upstream sides of the airframe with the wing. It should be noted that there is a good qualitative agreement and a small quantitative disagreement between the distributions of $C_p(\varphi)$ in the cross sections of objects 1 and 2.

The presence of the wing on the downstream side of the airframe causes a significant increase in the rarefaction on the airframe; however, the distribution of $C_p(\varphi)$ over this airframe agrees qualitatively with that of the isolated airframe. Here, the effect of the wing manifests itself as a displacement of the region of large pressure gradients $\partial C_p(\varphi)/\partial\varphi$ to the bourd chord of the wing. The calculation data (Figs. 4 and 5) obtained for the neighborhood of conjugation of the wing with the airframe on its upstream side differed most substantially. Unlike the isolated airframe, in all the cross sections x = const positioned on the conjugation line there arises a jump-like increase in the pressure due

Fig. 6. Lines of flow in the neighborhood of object 1.

to the shock wave induced by the wing panel. In this case, a local pressure maximum arises in the $C_p(\varphi)$ distribution as a result of the interaction of the shock wave induced by the wing with the airframe. In cross section 1^* (Figs. 4 and 5), this maximum arises at the point of conjugation of the wing with the airframe.

The intensity of the C_p maximum decreases downstream, and this maximum shifts to the generatrix $\varphi = 180^o$. The profile of the curve $C_p(\varphi)$ equalizes gradually from cross section to cross section, and the region of compression of the flow on the upstream side of the airframe widens. At the same time, the pressure at the airframe generatrix $\varphi = 180^o$ monotonically increases in the direction of the trailing edge, as compared with that of the isolated airframe. This marked difference between the indicated pressures in cross sections 3^* and 4^* is seen from Figs. 4 and 5.

We will now consider the following feature of a flow around object 1. The existence of a distorted leading shock wave as well as pointed edges and fractures on the surface of the airframe around which a stream flows is favorable for the formation of large-scale vortex structures. The form of these structures is mainly determined by the inertial forces. As was shown in [10], in this case it is not necessary that a viscous-medium model be used for simulation of the process of vortex formation.

The spatial pattern of a flow in the neighborhood of object 1 is shown in Fig. 6. Here, for illustration, the flow pattern is represented by a set of streamlines that are combined in "bands." The longitudinal twisting of bands points to the vortex formation in the distributed region. On the basis of calculation data, we separated and showed, in these figures, "bands" of streamlines originating on the upstream side of the leading shock wave and passing over the lower and upper surfaces of the wing. It should be noted that large-scale vortex structures are formed and develop in an eddying flow formed downstream of the distorted leading shock wave.

On the upstream side of the object (Fig. 6a), the streamlines smoothly pass over the lower surface and then leave the trailing edge. Large-scale vortices are formed when streamlines pass to the downstream side of the airframe and to the upper surface of the wing (Fig. 6). At the same time, vortex structures are intensively developed in the neighborhood of the line of conjugation of the wing with the airframe on its downstream side. It is seen from Fig. 6b that, in the indicated region, the "bands" of streamlines twist most intensively in the longitudinal direction.

The general dynamics of streamlines on the downstream side of the object and the tendency for the formation of a vortex sheet in the process of their propagation down from the trailing edge of the wing are shown in Fig. 6b. The data presented do not separate a vortex street downstream of the trailing edge of the wing.

Thus, based on the Euler equations, we have solved the problem on a supersonic flow around two configurations of a complex object consisting of an axisymmetric airframe and a triangular wing.

For construction of a high-level complex configuration, we proposed an algorithm of joining of its components. The compactness of the initial data necessary for construction of a complex geometric model allows one to rapidly change the aerodynamic geometry at the stage of preliminarily parametric investigations of the flow conditions.

Results of numerical calculation, at $M_\infty = 4.03$ and $\alpha = 10.1^o$, of a flow around an isolated ogival-cylindrical airframe, a wing, and an object composed of the airframe and wing in two variants are presented. Comparison of the data obtained for the isolated wing and air frame with analogous data obtained for the object composed of them has shown that the components of this object influence each other and determine the character of a flow around them and the distribution of loads over their surface. It is shown that the shift of the wing along the generatrix of the cylindrical

part of the airframe weakly influences the distribution of loads over the airframe and the wing. The calculation results were compared with the results of a physical experiment.

The author expresses his heartfelt gratitude to I. I. Mazhul', G. A. Tarnavskii, and A. A. Zheltovodov for usefull discussion and constant attention to the work.

NOTATION

b_0, length of the root chord of a wing, m; $C_w = y_{max}/L_z$, relative thickness of a profile; $C_{up} = y_{up}/L_z$, relative thickness of the upper part of the profile; $C_{low} = y_{low}/L_z$, relative thickness of the lower part of the profile; $C_p = (P - P_\infty)/q_\infty$, dimensionless pressure coefficient; D_m, diameter of the midsection of an airframe, m; E, total energy; e, specific internal energy; f, conservative parameters; $\mathbf{F}(g)$, vector of stream functions; g, gasdynamic parameters; $\mathbf{i}_1$, $\mathbf{i}_2$, $\mathbf{i}_3$, unit vectors of the Cartesian coordinate system; $L_z = x_i - x_k$, length of the local chord at z = const, m; M_∞, Mach number of the incident flow; M_n, normal component of the Mach number at the leading edge of the wing; $\mathbf{n}$, vector of the normal to the surface; P, static pressure, N/m^2; P_∞, static pressure of the incident flow, N/m^2; $q_\infty = \rho_\infty W_\infty^2/2$, kinetic head, N/m^2; $d\mathbf{S}$, vector of the area element of the surface of a cell; S, surface of a separated volume Ω; t, time; v_x, v_y, v_z, velocity-vector components $\mathbf{w}$; W_∞, velocity of the incident flow; x_i, coordinate of the trailing edge of the wing; $x_k = z/\tan\theta$, coordinate of the leading edge of the wing; $x_w = x/D_m$, coordinate of the origin of the bourd chord of the wing on the airframe; y_{up}, y_{low}, absolute values of the maximum thickness of the upper and lower profiles of the wing; z_{max}, local half-span of the wing in the cross section x = const; α, angle of attack; γ, adiabatic index; $\theta = \pi/2 - \chi$; $\lambda_h = L_h/D_m$, elongation of the head part of the airframe; $\lambda_c = L_c/D_m$, elongation of the cylindrical part of the airframe; $\mu = b/a$, ratio between the semiaxes of the hyperbolic function; ρ, density; χ, sweep angle; Ω, volume of a cell; $d\Omega$, element of the cell volume. Subscripts: up, upper surface of the wing; h, head part of the body; low, lower surface; c, cylindrical part of the body; m, midsection; max, maximum; n, normal component; ∞, parameters of the incident flow; w, wing.

REFERENCES

1. I. D. Faux and M. J. Pratt, *Computational Geometry for Design and Manufacture* [Russian translation], Mir, Moscow (1982).
2. N. F. Sevant, M. J. G. Bloor, and M. J. Wilson, Aerodynamic design of a flying wing using response surface methodology, *Aircraft*, **37**, No. 4, 562–569 (2000).
3. V. F. Volkov, Geometric modeling of complex configurations as applied to the problems of aerodynamics, *Vychislit. Metody Programmir.*, **2**, 112–122 (2001).
4. A. P. Shashkin and V. F. Volkov, A scheme for calculation of inviscid gasdynamic flows, in: *Problems of Flows Past 3-D Configurations* [in Russian], Collection of Sci. Papers of the Institute of Theoretical and Applied Mathematics of the Siberian Branch of the USSR Academy of Sciences, Novosibirsk (1978), pp. 17–56.
5. V. F. Volkov and I. I. Shabalin, A marching scheme of calculation of two-dimensional supersonic flows of inviscid gas, *Mat. Modelir.*, **10**, No. 2, 3–14 (1998).
6. V. F. Volkov, I. I. Mazhul', and D. V. Shcherbik, Calculation of supersonic inviscid gas flow past 3-D configurations with sharp leading edges, *Teplofiz. Aéromekh.*, **2**, No. 3, 245–252 (1995).
7. V. F. Volkov, A. A. Zheltovodov, and M. S. Loginov, Numerical simulation of supersonic inviscid gas flow past load-carrying structures, *Teplofiz. Aéromekh.*, **9**, No. 2, 217–232 (2002).
8. K. I. Babenko, G. P. Voskresenskii, A. I. Lyubimov, and V. V. Rusanov, *Spatial Ideal Gas Flow Past Smooth Bodies* [in Russian], Nauka, Moscow (1964).
9. L. G. Vasenev, Aerodynamic *Interference of a Wing and a Cylindrical Body at Supersound Speed*, Candidate Thesis (in Engineering), ITPM SO AN SSSR, Novosibirsk (1989).
10. V. F. Volkov, Numerical investigation of spatial flows in the vicinity of complex configurations, *Vychislit. Metody Programmir.*, **5**, 62–73 (2004).